Spectrochimica Acta Part A: Molecular and Biomolecular Spectroscopy 238 (2020) 118441

Contents lists available at ScienceDirect

Spectrochimica Acta Part A: Molecular and Biomolecular Spectroscopy

journal homepage: www.elsevier.com/locate/saa

Photoelectron spectra and electronic structure of boron diacetate formazanates

Sergey A. Tikhonov [a,*], Andrey E. Sidorin [a], Ilya S. Samoilov [b], Aleksandr V. Borisenko [c], Vitaliy I. Vovna [a]

[a] Far Eastern Federal University, School of Natural Sciences, Vladivostok 690950, Russian Federation
[b] Saint Petersburg State University, Department of Photonics, St. Petersburg 199034, Russian Federation
[c] Vladivostok Branch of Russian Customs Academy, Vladivostok 690034, Russian Federation

ARTICLE INFO

Article history:
Received 19 January 2020
Received in revised form 30 April 2020
Accepted 1 May 2020
Available online 05 May 2020

Keywords:
Electronic structure
Photoelectron spectroscopy
UPS
Density functional theory
Outer-valence Green's function (OVGF) method
Boron formazanate
Formazanate ligands

ABSTRACT

The electronic structure and cationic states of two 1,5-diphenylformazanes and two boron diacetate ($B(OAc)_2$) formazanates were modeled using the outer valence Green's function (OVGF) and density functional theory (DFT) methods. Comparison of data of the OVGF and ultraviolet photoelectron spectroscopy (UPS) methods made it possible to determine an effect of functional groups and complexing agents on energies of cationic states. Addition of NO_2-group at the γ-position of the chelate cycle causes stabilization of levels the five upper occupied molecular orbitals (MO) and destabilization of the bonding orbital $\pi_3^{Ph} + \pi_3$ level. The levels of MOs π_3^{Ph}–π_3 and n_- are stabilized due to influence of the complexing agent $B(OAc)_2$, with a difference in the shift of 0.67 eV. The ionization energies (I_n) changes for the π-orbitals of benzene rings are within the error of the OVGF method. Under methylation of phenyl groups, the differences between the calculated I_n, corresponding to the π-orbitals of aromatic substituents, are in good agreement with the experimental I_n shifts at transition from benzene to toluene. According to the OVGF method, in all the studied complexes the lowest unoccupied molecular orbital (LUMO) is localized mainly on the chelate cycle and has a strong acceptor character, which should contribute the low-lying charge-transfer electronic excitations. Moreover, an application of the DFT analog of the Koopmans' theorem with the BHHLYP and B2PLYP functionals made it possible to determine qualitatively a sequence of cationic states and energy intervals between them in the spectral range up to 10 eV. The DFT/wB97x/cc-pVTZ method data on the energy gap between the highest occupied molecular orbital (HOMO) and LUMO levels correlate with the OVGF/cc-pVTZ calculation results.

1. Introduction

Formazans are π-conjugated nitrogen-containing compounds that were first obtained >100 years ago [1] and initially attracted only sporadic attention. An interest in the coordination chemistry of boron formazanates has been growing recently, as these compounds are relatively easily synthesized and possess wide possibilities to control optical and redox properties [2–6], which makes them an excellent alternative to traditional BODIPY dyes. Materials based on boron formazanates can be used in biomedicine [7,8], polymer engineering [9,10], chemical technology [11], electrochemical analysis [12], and electrocatalysis [13].

At present, synthesis and physicochemical properties of boron formazanates are described in detail [14–18]. As well, a comprehensive assessment was made for results of modeling the structure and excited states of five compounds by the TDDFT, CIS(D), SOS-CIS(D), ADC(2), and CC2 methods [19]. However, nowadays there are extremely few experimental works [20] on detailed research of the electronic structure of boratetrazines and determination of the relationships "electronic structure – property". An identification of substitution effects and determination of relationships between the electronic structure of boron chelate complexes and their optical properties opens possibilities for controlled synthesis of new functional materials [21]. The most reliable data on the electronic structure of chemical compounds can be obtained by the combined application of the UPS method and quantum chemical calculations [22–24].

In order to determine the nature of overlapping bands in the photoelectron spectra of relatively small molecules, the calculation schemes based on the Green's function method [25–30] are successfully used. The OVGF method [31–34] is a third-order approximation and represents itself as a narrowly specialized approach to calculate transition energies to cationic states, which are well described in terms of the single-electron ionization for the upper valence orbitals. However, the OVGF method requires significant computational resources to model the ionized states of chelate complexes (n^5 with respect to the number of orbitals n). Therefore, the DFT analog of the Koopmans' theorem is often used in order to interpret the photoelectron spectra of boron coordination compounds [24]. In [35–38] it was shown that results of

* Corresponding author.
E-mail address: allser@bk.ru (S.A. Tikhonov).

https://doi.org/10.1016/j.saa.2020.118441
1386-1425/

calculations in the DFT approximation correlate well with the experimental ionization energies of boron chelates for the upper valence levels. That makes it possible to interpret unambiguously the photoelectron and optical spectra, as well as analyze the electronic effects of substitution.

This work presents the research results of the electronic structure and cationic states of two 1,5-diphenylformazanes and two $B(OAc)_2$ formazanates (Scheme 1) according to data of the UPS methods and to results of modeling the ionization processes by the OVGF and DFT methods.

2. Experimental and theoretical methods

UPS vapor spectra of compounds I–IV were obtained on a modified ES-3201 electronic spectrometer with a hemispherical electrostatic analyzer and a monochromatic radiation source (the radius of curvature of the trajectory was 100 mm, vacuum in analytical system was 10^{-4} Pa, the radiation energy was 21.22 eV (He (I)). An every-scan recording technique was introduced in this spectrometer, which made it possible to eliminate spectrum distortion during long-term accumulation (at least 50 scans with an accumulation duration of 100–500 ms in every of 1000 points) and monitor visually the mixture composition by the spectrum shape for every scan.

The samples were placed in the ionization chamber of an ES-3201 electronic spectrometer, where the required vapor pressure of ~10 Pa was reached by heating to 200–240 °C. Simultaneous heating of the substance and the whole energy-analyzer was done using quartz lamps (P = 1000 W). The ionization chamber temperature was controlled by the temperature sensor with an accuracy of 5 °C, and the volatility – by the intensity of UPS spectrum bands. Xenon ionization bands at 12.130 and 13.436 eV corresponding to the Xe $^2P_{3/2}$ and Xe $^2P_{1/2}$ lines, respectively, have been used as the calibrant bands.

The principal limits of the UPS method resolution were reviewed by D.W. Turner in [39]. These limits are caused by the broadening of lines in a light source and the thermal motion of ionized molecules, and they are approximately 0.005–0.010 eV. Many factors influence the working width of a spectral line: spectrometer aberrations, sizes of the input and output slit, scattered residual magnetic fields, heterogeneity of contact potential differences of the electronic path elements, instability of electric potentials of the control and registration systems. The error in determining the band maxima did not exceed 0.05 eV in the present work. The bands of the UPS spectra were interpreted taking into account the number of calculated electronic levels, energy intervals between them, and relative spectral intensities.

The optimal geometry search and calculations of the electronic structure of compounds I–IV by the DFT methods were carried out using the PC GAMESS v.16 software package [40]. Geometry of complexes in the state S_0 was optimized in the DFT approximation using the Def2-SVP basis set of atomic functions [41] and the B3LYP hybrid functional [42–44], which has been successfully applied to model the structure of boron coordination compounds [45–50]. In order to check compliance of the optimized structures with the local minimum points on the potential energy surface, the Hessian matrix was calculated.

Under interpreting the UPS spectra, as the reference data we used the results of calculations by the OVGF method with the cc-pVTZ basis set [51,52], obtained with the GAUSSIAN 16 software package [53]. Using acetylacetonate and bromoacetylacetonate of boron difluoride as examples, it was shown [54] that an application of the OVGF/cc-pVTZ method makes it possible to determine uniquely the nature of the UPS spectral bands of boron chelates. In addition, in order to compare the experimental values of the vertical I_n with the Kohn – Sham (KS) orbital energies ε_n, the DFT analog of the Koopmans' theorem was used [24]:

$$I_n = -\varepsilon_n + \delta,$$

where I_n is the ionization energy;

ε_n is the one-electron energy KS;

δ is a value of correction to the orbital energy.

The choice of the DFT method to model the cationic states is caused by the good correlation of experimental and theoretical ionization energies [24,35–38]. That is due to similarity of the KS equations and the quasiparticle Dyson's equation. It was shown in [55,56] that in the valence region the KS orbitals can be a good approximation of the Dyson orbitals [57], which are used to obtain the Green's functions [58]. DFT calculation results depend on a type of the exchange-correlation functional. At present, the hybrid functionals [59], double-hybrid functionals [60], Minnesota functionals [61], and range-separated functionals [62,63] are used for DFT calculations. According to the Hohenberg-Kohn theorems, the functional corresponds to the minimum energy if and only if the electron density, included in the functional, is the real density of the system in the ground state. For many years, development of the DFT methods has been focused on the energy accounting, i.e. the functionals corresponding to the lowest energies were considered as the best approximations of the exact functional. However, since the early 2000s, this trend has been reversed by the unconstrained functionals which sacrifice physical rigor to achieve the flexibility of empirical fit [64]. So, in the present work the results were analyzed only for 18 exchange-correlation functionals, which can be used to obtain qualitative results on distribution of the electron density of molecular systems [65].

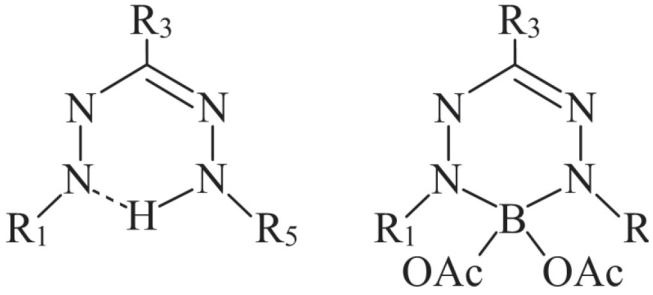

I. R_1=R_5=C_6H_5, R_3=H

II. R_1= R_5=C_6H_5, R_3=NO_2

III. R_1=R_5 =C_6H_5, R_3=H

IV. R_1=R_5 =*o*-$CH_3C_6H_5$, R_3=H

Scheme 1. Studied complexes I–IV.

3. Results and discussion

3.1. Electronic structure

Geometry optimization of the compounds I and II led to insignificant violations of coplanarity (about 1^0) of the planes of chelate and benzene rings, as well as to noticeable differences in the quasi-symmetric bond lengths and valence angles of the heterocycle (Scheme 1, Table S1 of ESI). At transition from I to II, no significant changes in geometric parameters are observed. The structures III and IV were modeled taking into account the C_S symmetry relative to the plane, which is perpendicular to the chelate cycle, according to experimental data on the crystal structure of the related compound [66]. In the compounds III and IV, the dihedral angles between planes of the chelate and phenyl groups are 26^0 and 48^0 respectively, and the angles between the N_α-C_R bond and the $N_\alpha N_\beta N_\beta N_\alpha$ plane are 10^0 and 14^0. Moreover, in the complexes III and IV, violation of the C_{2V} symmetry is caused by displacement of the complexing agent at the dihedral angles between the $N_\alpha BN_\alpha$ and $N_\alpha N_\beta N_\beta N_\alpha$ planes, which are 8^0 and 16^0 respectively.

Tables 1 and 2 present the experimental and calculated values of I_n, as well as contributions of orbitals of the chelate ring (A) and substituents (R_x) in the positions 1, 3, and 5 (Scheme 1) to molecular orbitals (MO) for compounds I–IV. The contributions of the Mulliken atomic populations are shown for the occupied orbitals, and the relative sums of squared coefficients of the basis orbitals are given for the vacant MOs. The π- and σ-orbitals of phenyl groups are indicated by the superscript "Ph", the MOs localized mainly on the complexing agent are denoted as $B(OAc)_2$. The orbitals are mixed if the sum of the Mulliken atomic populations for each fragment is >20%. The "+" sign denotes bonding, and "–" denotes anti-bonding. Shapes of some MOs are shown in Fig. 1. In order to demonstrate the electronic effects of substitution, Fig. 2 shows the correlation diagram I_n according to data of the calculation method OVGF/cc-pVTZ.

According to results of calculations by the OVGF/cc-pVTZ method, in the compound I, the I_1 at 7.37 eV corresponds to the anti-bonding combination of π-orbitals of benzene and chelate cycles (Table 1, Fig. 1), and the bonding orbital $\pi_3^{Ph} + \pi_3$ corresponds to I_6 (I_6–I_1 = 2.82 eV), which follows the MO n_- level (Fig. 1) and three π-orbitals of phenyl groups. The theoretical energy difference between I_6 and I_7 is 1.37 eV. In the range from 11.56 to 12.75 eV there are seven cationic states determined by photoionization processes from the MO with predominant contributions of the orbitals of benzene rings (Table 1).

Due to effect of the NO_2-group field (Table 3) in the γ-position (complex II), the stabilization by 0.26–0.56 eV is observed for levels of the four upper occupied MOs with predominant contributions of π-orbitals of benzene rings (Fig. 2, Table 1). The MO n_- level stabilization by 1.10 eV is determined by electron-acceptor properties of the substituent, which gets a part of the electron density (0.19 *e*) from the chelate cycle (Table 3). The $\pi_3 + \pi_3^{Ph}$ orbital level destabilization can be explained by influence of the orbitals of NO_2-group (Fig. 2).

Addition of the complexing agent (compound III) leads to stabilization of levels of the π_3^{Ph}–π_3 orbital by 0.35 eV and MO n_- by 1.02 eV relative to I (Tables 1 and 2). The significant difference in the shift value is determined by mixing of the MO n_- with the orbital localized mainly on $B(OAc)_2$. In the complex III, in comparison with I, due to effect of the complexing agent orbitals, the energy level for the bonding combination of π-orbitals of the benzene and chelate cycles, unlike the HOMO, is destabilized by 0.12 eV, which leads to a decrease in the difference I_n from the orbitals π_3^{Ph}–π_3 and $\pi_3^{Ph} + \pi_3$ from 2.82 to 2.35 eV. Changes of I_n from the π-orbitals of phenyl groups are within the OVGF method error.

A methylation of phenyl groups at the *p*-positions (compound IV) led to an increase in the theoretical value of I_1 by 0.18 eV relative to III (Table 2). At transition from III to IV, the changes in the calculated I_n, corresponded to the π-orbitals of phenyl groups, are in good agreement

Table 1
Localization of the highest occupied MOs (denoted as H, H–1, …) and the lowest vacant MOs (denoted as L), as well as the corresponding vertical ionization energies and electron affinities of compounds I–II according to the HF (Koopman's theorem) and OVGF methods.

MO, type	Contribution, %			Ionization energies, eV			Polestrength (OVGF)
	A	R_3	$R_1 + R_5$	HF	OVGF	Exptl data	
Compound I							
L, $\pi_4 + \pi_4^{Ph}$	66	0	34	−0.73	0.68	–	0.88
H, π_3^{Ph}–π_3	44	0	56	7.49	7.37	7.50	0.87
H–5, n_-	88	0	12	10.76	8.79		0.86
H–1, π_3^{Ph}	14	0	86	9.06	8.98	9.13	0.87
H–2, π_2^{Ph}	0	0	100	9.26	9.14		0.88
H–3, π_2^{Ph}	0	0	100	9.50	9.35		0.87
H–4, $\pi_3^{Ph} + \pi_3$	47	0	53	10.69	10.19	9.95	0.86
H–7, σ^{Ph} –n_+	42	3	55	13.21	11.56		0.86
H–6, π_1^{Ph}–π_2	27	0	73	13.17	11.98		0.81
H–8, σ^{Ph}	14	1	85	13.57	12.13		0.87
H–11, $\sigma^{Ph} + n_+$	28	1	71	14.05	12.44	11.98	0.86
H–10, σ^{Ph}	14	1	85	13.91	12.44		0.87
H–9, π_1^{Ph}	15	0	85	13.82	12.52		0.80
H–12, σ^{Ph}	9	1	90	14.25	12.75		0.87
H–13, $\pi_2 + \pi_1^{Ph}$	61	0	39	15.40	13.74	–	0.73
Compound II							
L, $\pi_4 + \pi_4^{Ph}$	68	2	30	−0.17	1.19	–	0.88
H, π_3^{Ph} –π_3	36	2	62	8.18	7.93	8.28	0.87
H–1, π_3^{Ph}	12	0	88	9.48	9.36		0.87
H–2, π_2^{Ph}	0	0	100	9.68	9.53		0.88
H–3, π_2^{Ph}	0	0	100	9.75	9.61	9.53	0.87
H–4, $n_- + \pi_3^{Ph}$	66	5	29	11.35	9.89		0.86
H–5, $\pi_3 + \pi_3^{Ph}$	66	4	30	11.37	9.95		0.86
H–6, NO_2	1	99	0	12.05	10.86	11.01	0.85
H–7, NO_2	8	90	2	13.19	11.03	–	0.86
H–8, NO_2	13	80	7	13.32	11.21	–	0.86

Table 2
Localization of the highest occupied MOs (denoted as H, H–1, …) and the lowest vacant MOs (denoted as L), as well as the corresponding vertical ionization energies and electron affinities of compounds III–IV according to the HF (Koopman's theorem) and OVGF methods.

MO, type	Contribution, %			Ionization energies, eV			Polestrength (OVGF)
	A	X	$R_1 + R_5$	HF	OVGF	Exptl data	
Compound III							
L, $\pi_4 + \pi_4^{Ph}$	76	1	23	−0.29	1.26	–	0.88
H, π_3^{Ph}–π_3	43	3	54	7.96	7.72	8.30	0.87
H–1, π_3^{Ph}	10	0	90	9.17	9.06	9.45	0.87
H–2, π_2^{Ph}	0	1	99	9.37	9.22		0.88
H–3, π_2^{Ph}	0	0	100	9.39	9.25		0.88
H–5, n_- + $B(OAc)_2$	60	28	12	11.73	9.81		0.86
H–4, $\pi_3^{Ph} + \pi_3$	44	4	52	10.68	10.07		0.86
H–6, $B(OAc)_2$	3	97	0	11.83	10.26		0.89
H–7, $B(OAc)_2$	0	99	1	12.20	10.59	10.77	0.89
H–8, $B(OAc)_2$	0	98	2	12.60	11.35	–	0.88
Compound IV							
L, $\pi_4 + \pi_4^{Ph}$	81	1	18	−0.59	1.03	–	0.88
H, π_3^{Ph} –π_3	44	3	53	8.20	7.90	8.02	0.87
H–1, π_3^{Ph}	3	0	97	8.96	8.82	9.47	0.88
H–2, π_2^{Ph}	1	0	99	9.09	8.94		0.88
H–3, π_2^{Ph}	4	1	95	9.20	9.03		0.88
H–5, n_- + $B(OAc)_2$	63	23	14	11.58	9.67		0.87
H–4, $\pi_3^{Ph} + \pi_3$	43	4	53	10.29	9.70		0.87
H–6, $B(OAc)_2$	2	98	0	11.83	10.23		0.89
H–7, $B(OAc)_2$	1	97	2	12.21	10.59	10.42	0.89
H–8, $B(OAc)_2$	0	95	5	12.54	11.24	–	0.88

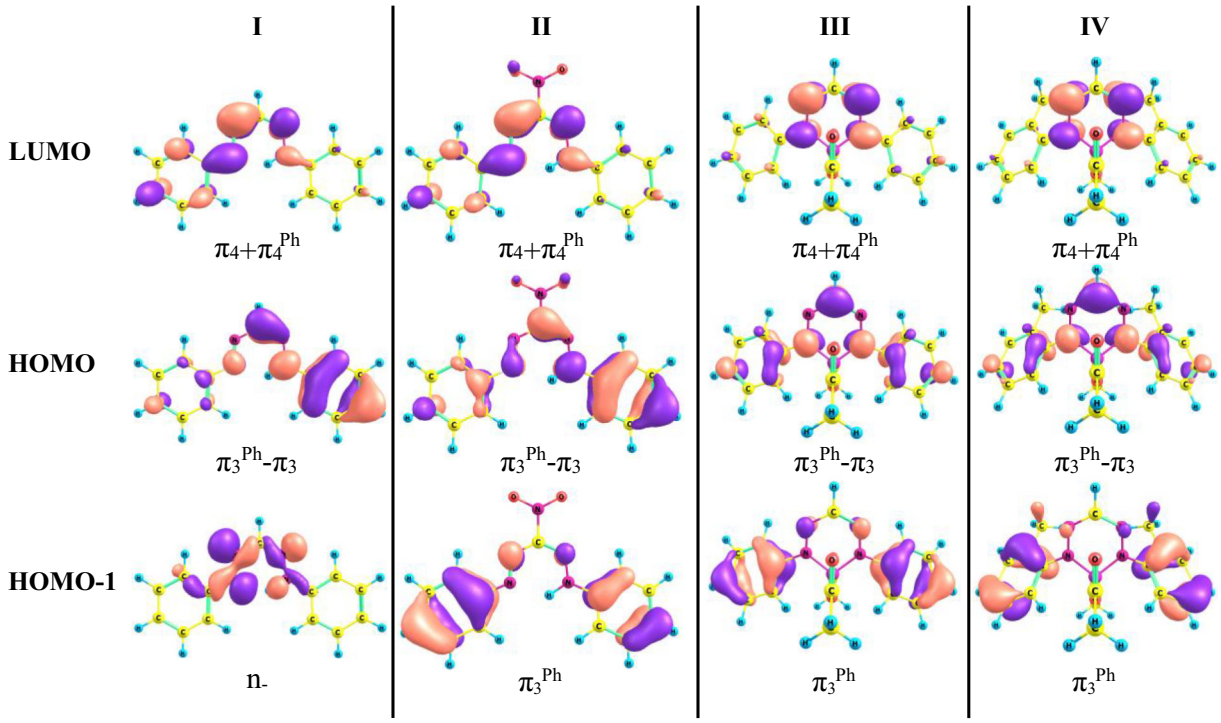

Fig. 1. Shapes of the LUMO and some upper occupied MOs of the compounds I–IV according to the HF/cc-pVTZ calculations.

with shifts of the experimental I_n at transition from benzene to toluene [23].

According to results of calculations by the OVGF/cc-pVTZ method, the LUMO in complexes I–IV is characterized by positive values of the electron affinity (E_{ea}), and the corresponding values of energies are in a range from 0.68 eV to 1.26 eV (Tables 1 and 2). That indicates that in the studied compounds the LUMO possesses a strong acceptor character, which facilitates low-lying electron excitations of the X-LUMO type, where X are various occupied MOs. In the complexes I–IV the LUMO is localized mainly on the chelate, and the orbitals of benzene rings are present among the upper occupied MOs. Therefore, part of bands in the absorption spectra of compounds I–IV should be determined by the transitions with electron density transfer from the substituent to the chelate cycle. That make it necessary to use the modern non-empirical methods for modeling the excited states of the studied molecules.

3.2. Photoelectron spectra

According to the OVGF/cc-pVTZ method, in the complex I UPS spectrum the band "1" at 7.50 eV is caused by ionization from the orbital π_3^{Ph}–π_3 (Fig. 3, Table 1). The broad band "2" at 9.13 eV corresponds to ionization processes from the chelate MO n– and three π-orbitals of phenyl groups. The band "3" at 9.95 eV is due to the cationic state with a hole on the MO, which is a bonding combination of the π orbitals of benzene and chelate rings. There are difficulties in interpreting the "4" band at 11.98 eV. First, the Xe $^2P_{3/2}$ line at 12.130 eV contributes to this band intensity. Second, for the three cationic states of compound I, the polestrength (P_n) values are observed being <0.85 (Table 1), which does not correspond to standard for the validity of valence ionization energies calculated with diagonal self-energy methods [67]. Perhaps, the states with energies 11.98, 12.52, and 13.74 eV have a complex configuration composition and cannot be interpreted as a result of ionization of one or another orbital, because at a decline in the fraction of the main (single-hole) configurations the values P_n decrease. I.e., there is a redistribution of intensity from the main photoelectron lines to the satellite lines, as well as a disturbance of the orbital ionization pattern [68]. In this case, in order to obtain reliable information, the more rigorous and resource-consuming ADC(3) method should be used [69,70].

The band "1" at 8.28 eV in the complex II UPS spectrum corresponds to the orbital π_3^{Ph}–π_3 (Fig. 3, Table 1). The broad band "2" at 9.53 eV goes next, it is determined by the ionization processes from three π-orbitals of benzene rings, the MOs $n_- + \pi_3^{Ph}$ and $\pi_3 + \pi_3^{Ph}$. The shoulder "3′" at 11.01 eV is due to the MO localized mainly on NO_2-group.

In the compound III UPS spectrum the band "1" at 8.30 eV is determined by photoionization processes from the MO π_3^{Ph}–π_3 (Fig. 4, Table 2). It should be noted that the I_1 calculated value differs from the experiment by 0.58 eV, which is noticeably larger than the expected value. As it was shown by calculations of values of the adiabatic and vertical I_1 based on a difference in the total energy (ΔE) between the ionized and ground states (DFT/CAMB3LYP/cc-pVTZ method), the ΔE value of complex III is increased by 0.38 eV relative to IV. That is caused by a deeper restructuring of the electron shell under the electron removal from the compound III HOMO and by an increase in the symmetry group from C_S to C_{2V}, which determines the ionization energy increase. In addition, the wide contour of the band "1" in the compound III spectrum indicates a significant change in the ion geometry under electron removal from the MOs, which are formally weakly bonding, in respect of their participation in the covalent bonding. Such large differences between the experimental and calculated I_1 values for compound III are probably due to properties of the determinant, which is used for calculations and represents a stable HF wave-function. The broad band "2" at 9.45 eV in the compound III spectrum corresponds to three π-orbitals of phenyl groups, MOs $n_- + B(OAc)_2$, $\pi_3^{Ph} + \pi_3$ and $B(OAc)_2$. The band "3" at 10.77 eV is caused by ionization from the orbital localized mainly on the complexing agent.

The band "1" at 8.02 eV in the complex IV UPS spectrum is due to ionization processes from the orbital π_3^{Ph}–π_3 (Fig. 4, Table 2). The band "2" at 9.47 eV is caused by ionization from three π-orbitals of the phenyl groups, MOs $n_- + B(OAc)_2$, $\pi_3^{Ph} + \pi_3$ and $B(OAc)_2$, and the band "3" at 10.42 eV corresponds to the orbital $B(OAc)_2$.

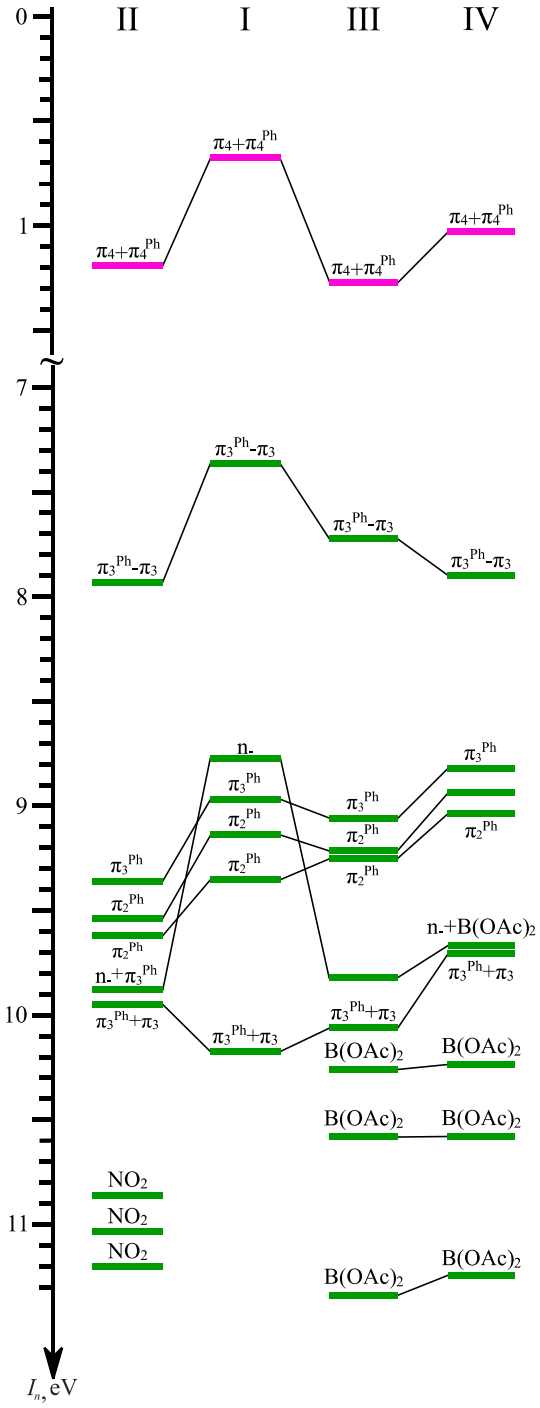

Fig. 2. A diagram correlating the lower unoccupied (*a*) and occupied (*b*) molecular orbitals of compounds I–IV based on the vertical ionization energies computed using the OVGF/cc-pVTZ.

3.3. Analysis of the results of DFT calculations

In order to evaluate the accuracy of modeling of cationic states using the DFT analog of the Koopmans' theorem, the experiment was correlated with the results of calculations with 18 different functionals (Table 4) which provide the most reliable data on distribution of the electron density of molecular systems [65]. The experimental energy intervals between maxima of the bands "1" and "3" were compared with the calculated energy differences between the corresponding electronic levels, the obtained differences were designated as ΔUPS. Moreover, the

Table 3
Total NBO charges (*e*) of the chelate cycle, complexing agent and substitutes.

Compd	A	X	R_1 + R_5	R_3
I	−0.51	+0.20	+0.20	+0.11
II	−0.32	+0.21	+0.24	−0.13
III	−0.44	+0.07	+0.26	+0.11
IV	−0.44	+0.07	+0.26	+0.11

values I_1–I_2 were compared for the OVGF and DFT methods, and the corresponding deviation values are denoted as ΔOVGF. The calculation methods in Table 4 are listed in an increasing order of ΔUPS. It should be noted that the results of calculations by the OVGF method depend on the version choice (A, B, C) [67,71]. In this work, the C version data are presented, because for the A and B versions, the noticeably large differences in the determination of the absolute ionization energies (Table S2 of ESI) are observed. The B version of the OVGF method is characterized by the overestimation of energy interval values.

At modeling the ionized states of arenes and molecules containing boron and nitrogen atoms, partial diagonal approaches P3 and P3+ [72–79] are used, which reproduce well the I_1 absolute values and the energy intervals between the bands "1" and "3" of UPS spectra of the

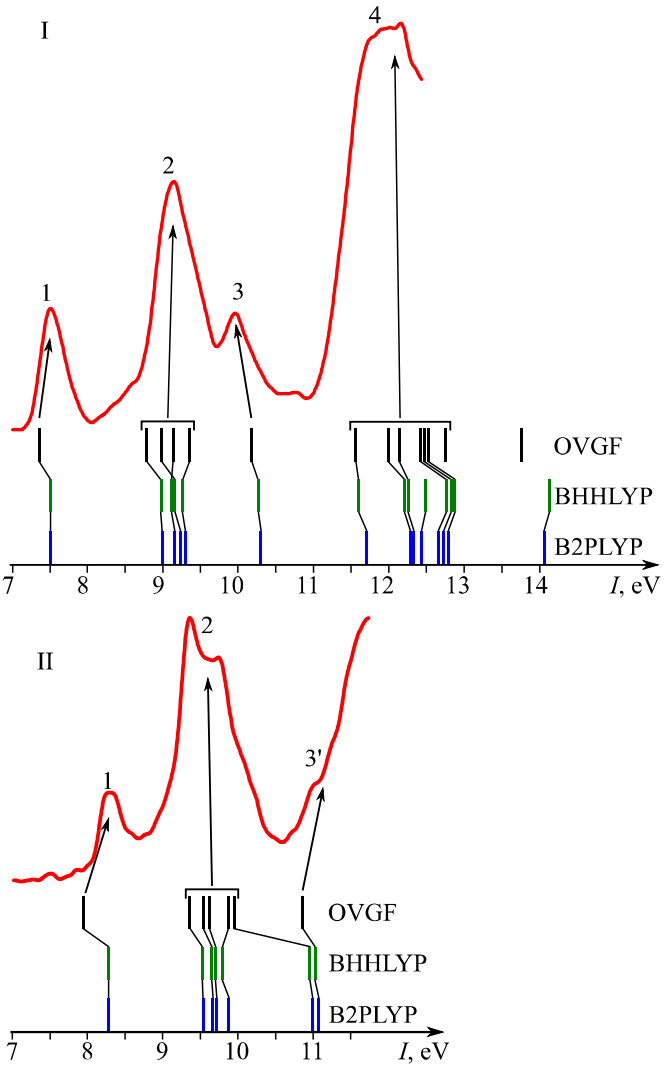

Fig. 3. Ultraviolet photoelectron spectra of vapors of the compounds I and II. The calculated ionization energies are shown by the vertical lines (OVGF/cc-pVTZ, DFT/BHHLYP/cc-pVTZ and DFT/B2PLYP/cc-pVTZ). For the DFT methods, the HOMO level position is correlated with the experimental value of I_1.

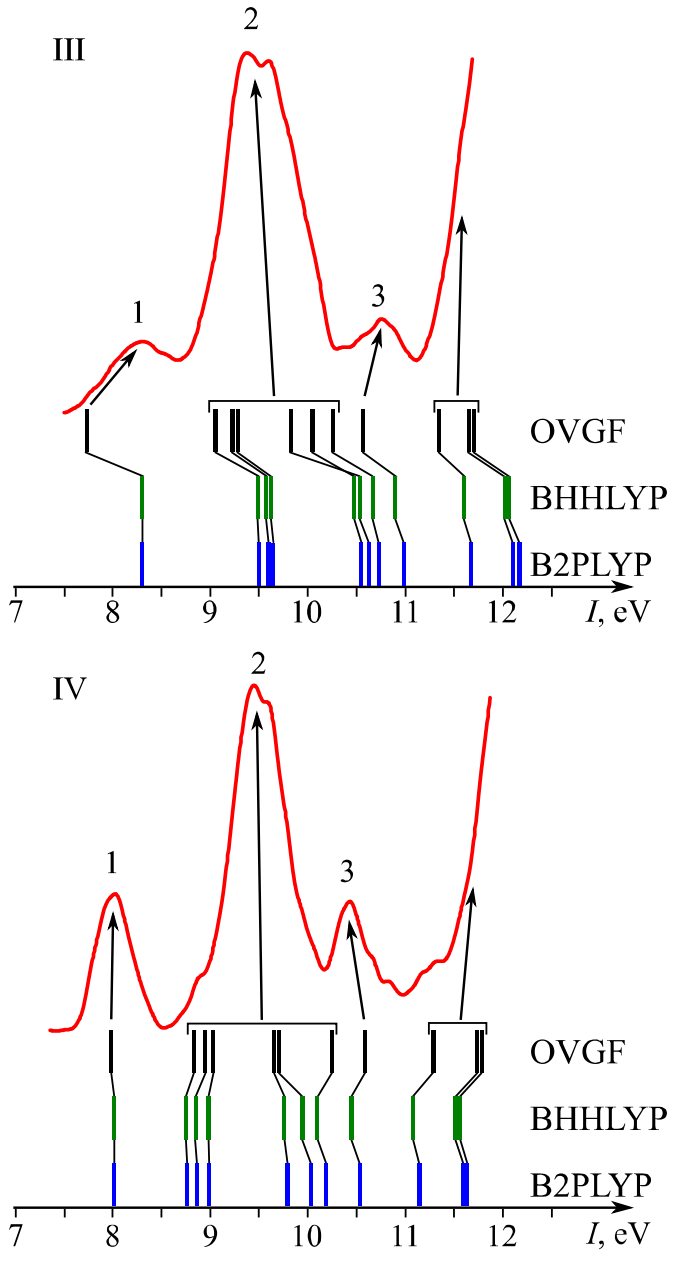

Fig. 4. Ultraviolet photoelectron spectra of vapors of the compounds III and IV. The calculated ionization energies are shown by the vertical lines (OVGF/cc-pVTZ, DFT/BHHLYP/cc-pVTZ and DFT/B2PLYP/cc-pVTZ). For the DFT methods, the HOMO level position is correlated with the experimental value of I_1.

compounds I–IV (Table S2 of ESI). However, for the methods P3 and P3+, the I_n calculation errors may be larger than for the OVGF method [71]. It is hard to correlate unambiguously the data of calculations by the methods P3 and P3+ with the experimental spectrum of the complex III (Fig. S1 of ESI), as well as for them the larger number of cationic states with $P_n < 0.85$ is observed in comparison with the results of the OVGF(C) method (Table S3 of ESI).

An analysis of the calculation results has shown that the application of DFT methods with the BHHLYP (hybrid GGA) [80], B2PLYP ("double hybrid" GGA) [81], and M06–2X (hybrid GGA) [82] functionals makes it possible to estimate the energy intervals between ionized states with the maximum absolute error (MAX AE) of 0.38 eV (Table 4), which is comparable with the MAX AE value of the OVGF method of 0.40 eV. It should be noted that the value of HF exchange for the above mentioned functionals exceeds 50%. For the wB97x [83], wB97 [83], and CAMB3LYP [84] range separated functionals, the value of MAX AE reaches 0.75 eV, and for the functionals with HF exchange up to 27%, the value of MAX AE exceeds 0.99 eV.

In a series of compounds II–IV for DFT calculations with the BHHLYP and B2PLYP functionals, the correlation is observed between the sequence of cationic states (in the energy range up to 10 eV) and the energy intervals between them (Figs. 3 and 4). The discrepancy between data of the OVGF and DFT methods (BHHLYP and B2PLYP functionals) for the sequence of complex I ionized states is caused by insignificant changes in the calculated energies, which are within the error of the OVGF/cc-pVTZ method. Compared to the BHHLYP and B2PLYP functionals, the M06-2X, wB97x, wB97, and CAMB3LYP functionals are characterized by noticeably larger differences from the OVGF method data (Figs. S2–S5 of ESI).

In a series of the studied complexes, the accuracy of the I_1 and E_{ea} calculations was estimated using the DFT analog of the Koopmans' theorem. The theoretical results for I_1 and E_{ea} were compared with the data of UPS (Table S4 of ESI) and OVGF (Table S5 of ESI) respectively. The use of the wB97x and wB97 range separated functionals made it possible to obtain the values I_1 with the MAX AE up to 0.43 eV (Table S4 of ESI). If consider the value of the OVGF method absolute error (AE) for I_1 of complex III, which is equal to 0.58 eV and caused by an increased relaxation energy, then the results of DFT calculations are inferior to the OVGF method accuracy. The MAX AE value for the CAMB3LYP, M06–2X, BHHLYP, and B2PLYP functionals reaches 1.43 eV, and for the rest 12 functionals it exceeds 1.94 eV. For DFT calculations with the wB97x and wB97 functionals, the Kohn – Sham LUMO energies are in good agreement with the E_{ea} according to the OVGF/cc-pVTZ method data, the MAX AE value is 0.18 eV (Table S5 of ESI). For the B2PLYP, CAMB3LYP, BHHLYP, and M06–2X functionals the MAX AE value reaches 1.32 eV, for the other functionals it exceeds 1.94 eV. According to Tables S4 and S5 of ESI, under a lack of computational resources, the use of the wB97x and wB97 range separated functionals is promising for estimation of the HOMO-LUMO energy gap of boron formazanates. Among the studied complexes, the maximum difference between the HOMO-LUMO energy gap values calculated by the DFT/wB97x/cc-pVTZ and DFT/wB97/cc-pVTZ methods is 0.60 and 0.90 eV, relative to OVGF/cc-pVTZ. Thus, the use of the wB97x functional makes it possible to calculate the energy gap under qualitative agreement with the OVGF/cc-pVTZ method data.

Comparison of the results of DFT calculations of the E_{ea} as a difference of the molecule total energies in the ground state and in the state with the attached electron has shown that for the M06–2X, wB97x, wB97, and CAMB3LYP functionals there is a good correlation (accuracy to 0.1 eV) with the OVGF data at a shift of 0.7 eV (Table S6 of ESI). The application of DFT methods for calculating the differences in the energies of molecules in the ground and ionized states did not provide satisfactory results for I_1.

4. Summary

According to calculations by the OVGF/cc-pVTZ method and the UPS data, the electronic substitution effects were revealed in a series of the four studied complexes, in which there is no influence of the functional groups on the HOMO and LUMO shapes. The field effect of NO_2-group in the γ-position determines the stabilization by 0.26–0.56 eV for levels of the four upper occupied MOs with the predominant contributions of the π-orbitals of phenyl groups. The orbital level n_- stabilization by 1.10 eV is caused by the electron-acceptor properties of NO_2-group, which gets the electron density (0.19 *e*) from the chelate cycle, and the $\pi_3^{Ph} + \pi_3$ level destabilization can be explained by effect of the substituent orbitals. The complexing agent addition leads to stabilization of the MO π_3^{Ph}–π_3 levels by 0.35 eV and the orbital n_- by 1.02 eV, the difference in the shift is determined by mixing of the MOs n_- and $B(OAc)_2$. The energy changes in I_n from the π-orbitals of phenyl groups are within errors of the OVGF/cc-pVTZ method. The addition of methyl groups at the *p*-

Table 4
Differences in the calculated energy intervals (eV) between I_1 and I_2, in comparison with the OVGF/cc-pVTZ method data (ΔOVGF). Differences between the experimental and calculated energy ranges between cationic states, which are correlated with the bands "1" and "3" of the UPS spectra (ΔUPS).

Method	AE								MAX AE	
	I		II		III		IV		ΔUPS	ΔOVGF
	ΔUPS	ΔOVGF	ΔUPS	ΔOVGF	ΔUPS	ΔOVGF	ΔUPS	ΔOVGF		
BHHLYP	0.31	−0.05	0.03	0.18	0.12	0.16	0.03	0.18	0.31	0.18
B2PLYP	0.35	−0.07	0.08	0.17	0.21	0.15	0.12	0.17	0.35	0.17
M06–2X	0.38	0.03	0.07	0.16	0.03	0.08	−0.08	0.11	0.38	0.16
OVGF	0.37	0.00	0.20	0.00	0.40	0.00	0.29	0.00	0.40	0.00
wB97x	0.48	0.06	−0.06	0.22	−0.36	0.04	−0.24	0.08	0.48	0.22
wB97	0.55	−0.05	0.02	0.12	−0.27	0.00	−0.16	0.05	0.55	0.12
CAMB3LYP	0.30	0.24	−0.24	0.41	−0.51	0.12	−0.75	0.15	0.75	0.41
B97–3	0.06	0.64	−0.54	0.80	−0.85	0.20	−0.99	0.20	0.99	0.80
PBE0	0.05	0.73	−0.61	0.89	−0.94	0.20	−1.06	0.21	1.06	0.89
X3LYP	−0.01	0.75	−0.66	0.92	−0.96	0.25	−1.08	0.23	1.08	0.92
B98	−0.01	0.76	−0.66	0.93	−0.98	0.24	−1.09	0.23	1.09	0.93
B97–1	−0.01	0.81	−0.69	0.98	−1.03	0.24	−1.13	0.22	1.13	0.98
B3LYPV3	−0.04	0.81	−0.70	0.99	−1.03	0.26	−1.13	0.24	1.13	0.99
B3LYP	−0.04	0.81	−0.70	0.99	−1.03	0.26	−1.13	0.24	1.13	0.99
B3P86V1R	−0.02	0.86	−0.71	1.03	−1.08	0.25	−1.16	0.23	1.16	1.03
B3P86	−0.02	0.87	−0.71	1.03	−1.08	0.24	−1.16	0.23	1.16	1.03
B3PW91	−0.02	0.88	−0.71	1.04	−1.09	0.24	−1.17	0.23	1.17	1.04
B97	−0.03	0.87	−0.73	1.04	−1.09	0.25	−1.18	0.23	1.18	1.04
tHCTHhyb	−0.10	1.00	−0.81	1.17	−1.22	0.33	−1.29	0.24	1.29	1.17

positions of aromatic substituents causes destabilization of the π-orbitals of phenyl groups by analogy with the shifts of the experimental I_n at transition from benzene to toluene.

According to the results of calculations by the OVGF/cc-pVTZ method, the E_{ea} values for all the studied compounds are positive in a range from 0.68 to 1.26 eV, which indicates a higher probability of low-lying electron excitations of the type X-LUMO, where X are various occupied MOs. Therefore, a part of bands in the absorption spectra of the studied complexes should be determined by the transitions with electron density transfer from the substituent to the chelate cycle, because the LUMO is localized mainly on the chelate cycle, and π-orbitals of benzene are present among the upper occupied MOs. That causes the necessity to use the modern non-empirical methods for modeling the excited states of $B(OAc)_2$ formazanates with aromatic substituents.

An analysis of the results of DFT calculations has shown that using the BHHLYP, B2PLYP, and M06–2X functionals with the HF exchange of >50%, as well as the wB97x, wB97, and CAMB3LYP range separated functionals, provide qualitative data on the energy intervals between cationic states of the studied complexes. In the energy range up to 10 eV the results of DFT calculations with the BHHLYP and B2PLYP functionals reproduce well the sequence of cationic states, in comparison with the OVGF/cc-pVTZ method data. Using the DFT analog of the Koopmans' theorem with an application of the wB97x and wB97 range separated functionals made it possible to obtain the absolute values I_1 and E_{ea} at the MAX AE up to 0.43 eV. Compared to the OVGF/cc-pVTZ data, the maximum difference between the HOMO-LUMO energy gap values according to the DFT/wB97x/cc-pVTZ method is 0.60 eV. That opens possibilities to calculate the HOMO-LUMO energy gap for boron formazanates under a lack of computing resources. Assessing the frontier of applicability of the above mentioned calculation methods for I_n and E_{ea} requires an analysis of a wider selection of research objects, which will be done in our further work.

CRediT authorship contribution statement

Sergey A. Tikhonov: Conceptualization, Methodology, Writing - original draft, Writing - review & editing, Validation. **Andrey E. Sidorin:** Resources, Investigation, Formal analysis, Visualization. **Ilya S. Samoilov:** Resources, Investigation. **Aleksandr V. Borisenko:** Resources, Investigation. **Vitaliy I. Vovna:** Resources, Supervision, Funding acquisition.

Declaration of competing interest

The authors declare that they have no known competing financial interests or personal relationships that could have appeared to influence the work reported in this paper.

Acknowledgements

This work was supported by the grants from the Ministry of Science and Higher Education of the Russian Federation (Grant No. 3.2168.2017/4.6, V.I.V. gratefully acknowledge Grant No. 16.5906.2017/6.7). Analysis of the results of DFT calculations was funded by RFBR according to the research project № 18-33-00197. Calculations of geometry and energies of MOs by the DFT method with various functionals were obtained using the equipment of Shared Resource Center "Far Eastern Computing Resource" IACP FEB RAS (https://cc.dvo.ru). Research was carried out using the GAUSSIAN 16 program [53] and computational resources provided by the "Computer Center of SPbU" Resource Center (http://cc.spbu.ru).

Appendix A. Supplementary data

Supplementary data to this article can be found online at https://doi.org/10.1016/j.saa.2020.118441.

References

[1] A.W. Nineham, The chemistry of formazans and tetrazolium salts, Chem. Rev. 55 (1955) 355–483.
[2] M.-C. Chang, E. Otten, Synthesis and ligand-based reduction chemistry of boron difluoride complexes with redox-active formazanate ligands, Chem. Commun. 50 (2014) 7431–7433.
[3] S.M. Barbon, P.A. Reinkeluers, J.T. Price, V.N. Staroverov, J.B. Gilroy, Structurally tunable 3-cyanoformazanate boron difluoride dyes, Chem. Eur. J. 20 (2014) 11340–11344.
[4] S.M. Barbon, V.N. Staroverov, J.B. Gilroy, Effect of extended π conjugation on the spectroscopic and electrochemical properties of boron difluoride formazanate complexes, J. Org. Chem. 80 (2015) 5226–5235.
[5] R.R. Maar, J.B. Gilroy, Aggregation-induced emission enhancement in boron difluoride complexes of 3-cyanoformazanates, J. Mater. Chem. C 4 (2016) 6478–6482.
[6] M.-C. Chang, A. Chantzis, D. Jacquemin, E. Otten, Boron difluorides with formazanate ligands: redox-switchable fluorescent dyes with large stokes shifts, Dalton Trans. 45 (2016) 9477–9484.
[7] R.R. Maar, S.M. Barbon, N. Sharma, H. Groom, L.G. Luyt, J.B. Gilroy, Evaluation of anisole-substituted boron difluoride formazanate complexes for fluorescence cell imaging, Chem. Eur. J. 21 (2015) 15589–15599.

[8] S.M. Barbon, S. Novoa, D. Bender, H. Groom, L.G. Luyt, J.B. Gilroy, Copper-assisted azide-alkyne cycloaddition chemistry as a tool for the production of emissive boron difluoride 3-cyanoformazanates, Org. Chem. Front. 4 (2017) 178–190.
[9] S. Novoa, J.B. Gilroy, (Co)polymers containing boron difluoride 3-cyanoformazanate complexes: emission enhancement via random copolymerization, Polym. Chem. 8 (2017) 5388–5395.
[10] J.S. Dhindsa, R.R. Maar, S.M. Barbon, M. Olivia Avilés, Z.K. Powell, F. Lagugné-Labarthet, J.B. Gilroy, A π-conjugated inorganic polymer constructed from boron difluoride formazanates and platinum(ii) diynes, Chem. Commun. 54 (2018) 6899–6902.
[11] S.M. Barbon, V.N. Staroverov, J.B. Gilroy, Structurally diverse boron-nitrogen heterocycles from an N2O23− formazanate ligand, Angew. Chem. Int. Ed. 56 (2017) 8173–8177.
[12] M. Hesari, S.M. Barbon, V.N. Staroverov, Z. Ding, J.B. Gilroy, Efficient electrochemiluminescence of a readily accessible boron difluoride formazanate dye, Chem. Commun. 51 (2015) 3766–3769.
[13] R. Mondol, E. Otten, Reactivity of two-electron-reduced boron formazanate compounds with electrophiles: facile N-H/N-C bond homolysis due to the formation of stable ligand radicals, Inorg. Chem. 57 (2018) 9720–9727.
[14] M. Hesari, S.M. Barbon, R.B. Mendes, V.N. Staroverov, Z. Ding, J.B. Gilroy, Structural tuning of boron difluoride formazanate electrochemiluminescence mediated by tri-n-propylamine, J. Phys. Chem. C 122 (2018) 1258–1266.
[15] G.N. Lipunova, T.G. Fedorchenko, O.N. Chupakhina, New aspects of the chemistry of formazans, Russ. J. Gen. Chem. 89 (2019) 1225–1245.
[16] A.V. Belois, R.R. Maar, M.S. Workentin, J.B. Gilroy, Dialkynylborane complexes of formazanate ligands: synthesis, electronic properties, and reactivity, Inorg. Chem. 58 (2019) 834–843.
[17] R.R. Maar, N.A. Hoffman, V.N. Staroverov, J.B. Gilroy, Oxoborane formation turns on formazanate-based photoluminescence, Chem. Eur. J. 25 (2019) 11015–11019.
[18] R.R. Maar, R. Zhang, D.G. Stephens, Z. Ding, J.B. Gilroy, Near-infrared photoluminescence and electrochemiluminescence from an exceptionally simple boron difluoride formazanate dye, Angew. Chem. Int. Ed. 58 (2019) 1052–1056.
[19] A.D. Laurent, E. Otten, B. Le Guennic, D. Jacquemin, Formazanate boron difluoride dyes: discrepancies between TD-DFT and wavefunction descriptions, J. Mol. Model. 22 (2016) 263–270.
[20] S.A. Tikhonov, V.I. Vovna, A.V. Borisenko, Photoelectron spectra and electronic structure of nitrogen analogues of boron β-diketonates with aromatic substituents, J. Electron Spectr. Relat. Phenom. 213 (2016) 32–38.
[21] M. Ponce-Vargas, B. Štefane, E. Zaborova, F. Fages, A. D'Aléo, D. Jacquemin, B. Le Guennic, Searching for new borondifluoride β-diketonate complexes with enhanced absorption/emission properties using ab initio tools, Dyes Pigments 155 (2018) 59–67.
[22] V.I. Nefedov, V.I. Vovna, Electronic Structure of Chemical Compounds, Nauka, Moscow, 1987 (in Russian).
[23] V.I. Nefedov, V.I. Vovna, Electronic Structure of Organic and Organoelement Compounds, Nauka, Moscow, 1989 (in Russian).
[24] I.S. Osmushko, V.I. Vovna, S.A. Tikhonov, Y.V. Chizhov, I.V. Krauklis, Application of DFT for the modeling of the valence region photoelectron spectra of boron and d-element complexes and macromolecules, Int. J. Quantum Chem. 116 (2016) 325–332.
[25] L.S. Cederbaum, One-body Green's function for atoms and molecules: theory and application, J. Phys. B 8 (1975) 290–303.
[26] L.S. Cederbaum, W. Domcke, in: I. Prigogine, S.A. Rice (Eds.), Advances in Chemical Physics, 36, Wiley & Sons, New York 1977, p. 205.
[27] J.V. Ortiz, Electron binding energies of anionic alkali metal atoms from partial fourth order electron propagator theory calculations, J. Chem. Phys. 89 (1988) 6348–6352.
[28] J.V. Ortiz, Partial fourth order electron propagator theory, Int. J. Quantum Chem., Quant. Chem. Symp. 34 (S22) (1988) 431–436.
[29] J.V. Ortiz, Partial third-order quasiparticle theory: comparisons for closed-shell ionization energies and an application to the Borazine photoelectron spectrum, J. Chem. Phys. 104 (1996) 7599–7605.
[30] A.B. Trofimov, J. Schirmer, V.B. Kobychev, A.W. Potts, D.M.P. Holland, L. Karlsson, Photoelectron spectra of the nucleobases cytosine, thymine and adenine, J. Phys. B Atomic Mol. Phys. 39 (2006) 305–326.
[31] W. von Niessen, J. Schirmer, L.S. Cederbaum, Computational methods for the one-particle Green's function, Comp. Phys. Rep. 1 (1984) 57–125.
[32] V.G. Zakrzewski, J.V. Ortiz, Semidirect algorithms in electron propagator calculations, Int. J. Quantum Chem., Quant. Chem. Symp. (S28) (1994) 23–27.
[33] J.V. Ortiz, V.G. Zakrzewski, O. Dolgounircheva, in: J.-L. Calais, E. Kryachko (Eds.), Conceptual Perspectives in Quantum Chemistry, Kluwer Academic, Dordrecht 1997, pp. 465–518.
[34] A.M. Ferreira, G. Seabra, O. Dolgounitcheva, V.G. Zakrzewski, J.V. Ortiz, Quantum-mechanical prediction of thermochemical data, in: J. Cioslowski (Ed.), Understanding Chemical Reactivity, 22, Kluwer Academic, Dordrecht 2001, pp. 131–160.
[35] S.A. Tikhonov, V.I. Vovna, Boron chelate complexes: X-ray and UV photoelectron spectra and electronic structure, Russ. Chem. Bull. 67 (2018) 1153–1166.
[36] S.A. Tikhonov, I.V. Svistunova, I.S. Samoilov, I.S. Osmushko, A.V. Borisenko, V.I. Vovna, Electronic structure of binuclear acetylacetonates of boron difluoride, J. Mol. Struct. 1160 (2018) 92–100.
[37] S.A. Tikhonov, V.I. Vovna, I.B. L'vov, I.S. Os'mushko, A.V. Borisenko, E.V. Fedorenko, A.G. Mirochnik, Electronic structure and optical properties of boron difluoride naphthaloyl- and anthracenoylacetonates, J. Lumin. 195 (2018) 79–86.
[38] S.A. Tikhonov, E.V. Fedorenko, A.G. Mirochnik, I.S. Osmushko, A.D. Skitnevskaya, A.B. Trofimov, V.I. Vovna, Spectroscopic and quantum chemical study of difluoroboron b-diketonate luminophores: isomeric acetylnaphtholate chelates, Spectrochim. Acta Mol. Biomol. Spectrosc. 214 (2019) 67–78.
[39] D.W. Turner, C. Baker, A.D. Baker, C.R. Brundle, Molecular Photoelectron Spectroscopy, Wiley-Interscience, New York, 1970 386.
[40] M.W. Schmidt, K.K. Baldridge, J.A. Boatz, S.T. Elbert, M.S. Gordon, J.H. Jensen, S. Koseki, N. Matsunaga, K.A. Nguyen, S.J. Su, T.L. Windus, M. Dupuis, J.A. Montgomery, General atomic and molecular electronic structure system, J. Comput. Chem. 14 (1993) 1347–1363.
[41] F. Weigend, R. Ahlrichs, Balanced basis sets of split valence, triple zeta valence and quadruple zeta valence quality for H to Rn: design and assessment of accuracy, Phys. Chem. Chem. Phys. 7 (2005) 3297–3305.
[42] C. Lee, W. Yang, R.G. Parr, Development of the Colle-Salvetti correlation-energy formula into a functional of the electron density, Phys. Rev. B: Condens. Matter Mater. Phys. 37 (1988) 785–789.
[43] A.D. Becke, Density-functional thermochemistry. III. The role of exact exchange, J. Chem. Phys. 98 (1993) 5648–5652.
[44] P.J. Stephens, F.J. Devlin, C.F. Chabalowski, M.J. Frisch, Ab initio calculation of vibrational absorption and circular dichroism spectra using density functional force fields, J. Phys. Chem. 98 (1994) 11623–11627.
[45] G.B. Guseva, E.V. Antina, A.A. Ksenofontov, E.N. Nuraneeva, A quantum chemical study of the molecular structure of zinc(II) and boron(III) complexes with monoiodo and dibromo substituted dipyrrines, J. Struct. Chem. 57 (2016) 25–32.
[46] D.N. Tomilin, K.B. Petrushenko, L.N. Sobenina, M.D. Gotsko, I.A. Ushakov, A.D. Skitnevskaya, A.B. Trofimov, B.A. Trofimov, Synthesis and optical properties of meso-CF3-BODIPY with acylethynyl substituents in the 3-position of the indacene core, Asian J. Org. Chem. 5 (2016) 1288–1294.
[47] H. Zhang, C. Liu, J. Xiu, J. Qiu, Triphenylamine-modified difluoroboron dibenzoylmethane derivatives: synthesis, photophysical and electrochemical properties, Dyes Pigments 136 (2017) 798–806.
[48] D.A. Merkushev, S.D. Usoltsev, Yu.S. Marfin, A.P. Pushkarev, D. Volyniuk, J.V. Grazulevicius, E.V. Rumyantsev, BODIPY associates in organic matrices: spectral properties, photostability and evaluation as OLED emitters, Mater. Chem. Phys. 187 (2017) 104–111.
[49] Y. Bai, X. Shi, Y. Chen, C. Zhu, Y. Jiao, Z. Han, W. He, Z. Guo, Coumarin/BODIPY hybridisation for ratiometric sensing of intracellular polarity oscillation, Chem. Eur. J. 24 (2018) 7513–7524.
[50] Y. Hisamune, T. Kim, K. Nishimura, M. Ishida, M. Toganoh, S. Mori, D. Kim, H. Furuta, Switch-ON near IR fluorescent dye upon protonation: helically twisted bis(boron difluoride) complex of π-extended corrorin, Chem. Eur. J. 24 (2018) 4628–4634.
[51] T.H. Dunning, Gaussian basis sets for use in correlated molecular calculations. I. The atoms boron through neon and hydrogen, J. Chem. Phys. 90 (1989) 1007–1023.
[52] R.A. Kendall, T.H. Dunning, R.J. Harrison, Electron affinities of the first-row atoms revisited. Systematic basis sets and wave functions, J. Chem. Phys. 96 (1992) 6796–6806.
[53] M.J. Frisch, G.W. Trucks, H.B. Schlegel, G.E. Scuseria, M.A. Robb, J.R. Cheeseman, G. Scalmani, V. Barone, G.A. Petersson, H. Nakatsuji, X. Li, M. Caricato, A.V. Marenich, J. Bloino, B.G. Janesko, R. Gomperts, B. Mennucci, H.P. Hratchian, J.V. Ortiz, A.F. Izmaylov, J.L. Sonnenberg, D. Williams-Young, F. Ding, F. Lipparini, F. Egidi, J. Goings, B. Peng, A. Petrone, T. Henderson, D. Ranasinghe, V.G. Zakrzewski, J. Gao, N. Rega, G. Zheng, W. Liang, M. Hada, M. Ehara, K. Toyota, R. Fukuda, J. Hasegawa, M. Ishida, T. Nakajima, Y. Honda, O. Kitao, H. Nakai, T. Vreven, K. Throssell, J.A. Montgomery Jr., J.E. Peralta, F. Ogliaro, M.J. Bearpark, J.J. Heyd, E.N. Brothers, K.N. Kudin, V.N. Staroverov, T.A. Keith, R. Kobayashi, J. Normand, K. Raghavachari, A.P. Rendell, J.C. Burant, S.S. Iyengar, J. Tomasi, M. Cossi, J.M. Millam, M. Klene, C. Adamo, R. Cammi, J.W. Ochterski, R.L. Martin, K. Morokuma, O. Farkas, J.B. Foresman, D.J. Fox, Gaussian 16, Revision B.01, Gaussian, Inc, Wallingford CT, 2016.
[54] S.A. Tikhonov, I.S. Samoilov, I.V. Krauklis, A.V. Borisenko, V.I. Vovna, Photoelectron spectra and electronic structure of acetylacetonate and bromoacetylacetonate of boron difluoride, J. Phys. Conf. Ser. 1172 (2019) 12013.
[55] S. Hamel, P. Duffy, M.E. Casida, D.R. Salahub, Kohn-Sham orbitals and orbital energies: fictitious constructs but good approximations all the same, J. Electron Spectrosc. Relat. Phenom. 123 (2002) 345–363.
[56] P. Duffy, D.P. Chong, M.E. Casida, D.R. Salagub, Assessment of Kohn-Sham density-functional orbitals as approximate Dyson orbitals for the calculation of electron-momentum-spectroscopy scattering cross sections, Phys. Rev. A: At. Mol. Opt. Phys. 50 (1994) 4707–4728.
[57] E.K.U. Gross, E. Runge, O. Heinonen, Many Particle Theory, Adam Hilger, Bristol, U.K, 1992.
[58] E.N. Economou, Green's Functions in Quantum Physics, Springer, New York, 1979.
[59] M. Marsman, J. Paier, A. Stroppa, G. Kresse, Hybrid functionals applied to extended systems, J. Phys. Condens. Matter 20 (2008) 64201.
[60] L. Goerigk, S. Grimme, Double-hybrid density functional, Wiley Interdiscip. Rev.: Comput. Mol. Sci. 4 (2014) 576–600.
[61] Y. Zhao, D.G. Truhlar, Applications and validations of the Minnesota density functional, Chem. Phys. Lett. 502 (2011) 1–13.
[62] A.E. Raeber, B.M. Wong, The importance of short- and longrange exchange on various excited state properties of DNA monomers, stacked complexes, and Watson-Crick pairs, J. Chem. Theory Comput. 11 (2015) 2199–2209.
[63] A. Prlj, B.F.E. Curchod, A. Fabrizio, L. Floryan, C. Corminboeu, Qualitatively incorrect features in the TDDFT spectrum of thiophene-based compounds, J. Phys. Chem. Lett. 6 (2015) 13–21.
[64] M.G. Medvedev, I.S. Bushmarinov, J. Sun, J.P. Perdew, K.A. Lyssenko, Density functional theory is straying from the path toward the exact functional, Science (6320) (2017) 49–52.
[65] K.R. Brorsen, Y. Yang, M.V. Pak, S. Hammes-Schiffer, Is the accuracy of density functional theory for atomization energies and densities in bonding regions correlated? J. Phys. Chem. Lett. 8 (2017) 2076–2081.

[66] J.B. Gilroy, M.J. Ferguson, R. McDonald, B.O. Patrick, R.G. Hicks, Formazans as b-diketiminate analogues. Structural characterization of boratatetrazines and their reduction to borataverdazyl radical anions, Chem. Commun. 126 (2007) 126–128.
[67] J.V. Ortiz, Electron propagator theory: an approach to prediction and interpretation in quantum chemistry, Wiley Interdiscip. Rev. Comput. Mol. Sci. 3 (2013) 123–142.
[68] L.S. Cederbaum, W. Domcke, J. Schirmer, W. von Niessen, Correlation effects in the ionization of molecules: breakdown of the molecular orbital picture, Adv. Chem. Phys. 65 (1986) 115–159.
[69] J. Schirmer, L.S. Cederbaum, O. Walter, New approach to the one-particle Green's function for finite Fermi systems, Phys. Rev. A 28 (1983) 1237–1259.
[70] I.L. Zaytseva, A.B. Trofimov, J. Schirmer, O. Plekan, V. Feyer, R. Richter, M. Coreno, K.C. Prince, Theoretical and experimental study of valence-shell ionization spectra of guanine, J. Phys. Chem. A 113 (2009) 15142–15149.
[71] H.H. Corzo, J.V. Ortiz, Electron Propagator Theory: Foundations and Predictions, 74, Academic Press, Elsevier, Cambridge, MA, 2017 267–298.
[72] H.H. Corzo, A. Galano, O. Dolgounitcheva, V.G. Zakrzewski, J.V. Ortiz, NR2 and P3+: accurate, efficient electron-propagator methods for calculating valence, vertical ionization energies of closed-shell molecules, J. Phys. Chem. A 119 (2015) 8813–8821.
[73] O. Dolgounitcheva, M. Díaz-Tinoco, V.G. Zakrzewski, R.M. Richard, N. Marom, C.D. Sherrill, J.V. Ortiz, Accurate ionization potentials and electron affinities of acceptor molecules IV: electron-propagator methods, J. Chem. Theory Comput. 12 (2016) 627–637.
[74] M. Díaz-Tinoco, J.V. Ortiz, Carborane superhalide bases and their conjugate Brønsted-Lowry Superacids: electron binding energies and Dyson orbitals, Chem. Phys. 521 (2019) 77–84.
[75] S.X. Tian, Ab initio and electron propagator theory study of boron hydrides, J. Phys. Chem. A 109 (2005) 5471–5480.
[76] J.V. Ortiz, Electron propagator theory of the ground and excited states of calcium borohydride, J. Am. Chem. Soc. 113 (1991) 1102–1108.
[77] J.V. Ortiz, Electron propagator theory of BS2 and BS−2 electronic structure, Chem. Phys. Lett. 214 (1993) 467–472.
[78] G. Seabra, V.G. Zakrzewski, J.V. Ortiz, Electron propagator theory of ionization energies and dyson orbitals for μ-hydrido, bridge-bonded molecules: diborane, digallane, and gallaborane, ACS Symp. Ser. Am. Chem. Soc. 827 (2002) 118–134.
[79] M. Díaz-Tinoco, O. Dolgounitcheva, V.G. Zakrzewski, J.V. Ortiz, Composite electron propagator methods for calculating ionization energies, J. Chem. Phys. 144 (2016), 224110. .
[80] A.D. Becke, A new mixing of Hartree-Fock and local density-functional theories, J. Chem. Phys. 98 (1993) 1372–1377.
[81] S. Grimme, Semiempirical hybrid density functional with perturbative second-order correlation, J. Chem. Phys. 124 (2006), 034108. .
[82] Y. Zhao, D.G. Truhlar, The M06 suite of density functionals for main group thermochemistry, thermochemical kinetics, noncovalent interactions, excited states, and transition elements: two new functionals and systematic testing of four M06-class functionals and 12 other functionals, Theor. Chem. Accounts 120 (2008) 215–241.
[83] J.-D. Chai, M. Head-Gordon, Systematic optimization of long-range corrected hybrid density functionals, J. Chem. Phys. 128 (2008), 084106. .
[84] T. Yanai, D. Tew, N. Handy, A new hybrid exchange-correlation functional using the Coulomb-attenuating method (CAM-B3LYP), Chem. Phys. Lett. 393 (2004) 51–57.